

Constraining  $M_\nu$  with the Bispectrum II: the Information Content of the Galaxy BispectrumCHANGHOON HAHN,<sup>1,2,\*</sup> FRANCISCO VILLAESCUSA-NAVARRO,<sup>3,4</sup> AND ...<sup>1</sup>*Lawrence Berkeley National Laboratory, 1 Cyclotron Rd, Berkeley CA 94720, USA*<sup>2</sup>*Berkeley Center for Cosmological Physics, University of California, Berkeley, CA 94720, USA*<sup>3</sup>*Center for Computational Astrophysics, Flatiron Institute, 162 5th Avenue, New York, NY 10010, USA*<sup>4</sup>*Department of Astrophysical Sciences, Princeton University, Peyton Hall, Princeton NJ 08544, USA*

(Dated: DRAFT --- 014469f --- 2020-07-09 --- NOT READY FOR DISTRIBUTION)

## ABSTRACT

Massive neutrinos suppress the growth of structure on small scales and leave an imprint on large-scale structure that can be measured to constrain their total mass,  $M_\nu$ . With standard analyses of two-point clustering statistics,  $M_\nu$  constraints are severely limited by parameter degeneracies. [Hahn et al. \(2020\)](#) demonstrated that the bispectrum, the next higher-order statistic, can break these degeneracies and dramatically improve constraints on  $M_\nu$  and other cosmological parameters. In this paper, we present the constraining power of the redshift-space *galaxy* bispectrum,  $B_0^g$ . We construct 195,000 mock galaxy catalogs from the QUIJOTE  $N$ -body simulation suite using the halo occupation distribution (HOD) model, which provides an effective galaxy bias framework well-suited for simulation-based approaches. Using these mocks, we present the Fisher matrix forecasts of  $\{\Omega_m, \Omega_b, h, n_s, \sigma_8, M_\nu\}$  and quantify, for the first time, the total information content of the  $B_0^g$  down to nonlinear scales. For  $k_{\text{max}}=0.5 h/\text{Mpc}$ ,  $B_0^g$  improves constraints on  $\Omega_m, \Omega_b, h, n_s, \sigma_8$  by **CH: 3.3, 3.6, 4.5, 4.9, and  $4.7\times$**  over power spectrum, even after marginalizing over HOD parameters. For  $M_\nu$ , we derive  $5.6\times$  tighter constraints with  $B_0^g$ . Even with priors from *Planck*,  $B_0^g$  improves cosmological constraints by **CH:  $\gtrsim 2\times$** . While effects such as survey geometry and assembly bias will have an impact, these constraints are derived for  $(1 h^{-1}\text{Gpc})^3$ , a substantially smaller volume than upcoming surveys. Therefore, we conclude that including the galaxy bispectrum will significantly improve cosmological constraints, especially  $M_\nu$ , for upcoming galaxy surveys.

*Keywords:* cosmology: cosmological parameters — cosmology: large-scale structure of Universe. — cosmology: theory

## 1. INTRODUCTION

\* hahn.changhoon@gmail.com

More than two decades ago, neutrino oscillation experiments discovered the lower bound on the sum of neutrino masses ( $M_\nu \gtrsim 0.06$  eV) and confirmed physics beyond the Standard Model (Fukuda et al. 1998; Forero et al. 2014; Gonzalez-Garcia et al. 2016). Since then, experiments have sought to more precisely measure  $M_\nu$  in order to distinguish between the ‘normal’ and ‘inverted’ neutrino mass hierarchy scenarios and further reveal the physics of neutrinos. Upcoming laboratory experiments (*e.g.* double beta decay and tritium beta decay), however, will not be sufficient to distinguish between the mass hierarchies (Bonn et al. 2011; Drexlin et al. 2013). Fortunately, complementary and more precise constraints on  $M_\nu$  can be placed by measuring the effect of neutrinos on the expansion history and growth of cosmic structure.

In the early Universe, neutrinos are relativistic and contribute to the energy density of radiation. Later, as they become non-relativistic, they contribute to the energy density of matter. This transition affects the expansion history of the Universe and leaves imprints on the cosmic microwave background (CMB Lesgourgues & Pastor 2012, 2014). Massive neutrinos also impact the growth of structure. While neutrino perturbations are indistinguishable from cold dark matter (CDM) perturbations on large scales, but below their free-streaming scale, neutrinos do not contribute to the clustering and reduce the amplitude of the total matter power spectrum. They also reduce the growth rate of CDM perturbations at late times. This combined suppression of the small-scale matter power spectrum leaves measurable imprints on the CMB as well as large-scale structure (for further details see Lesgourgues & Pastor 2012, 2014; Gerbino 2018).

The tightest cosmological constraints on  $M_\nu$  currently come from combining CMB temperature and large angle polarization data from the *Planck* satellite with Baryon Acoustic Oscillation and CMB lensing:  $M_\nu < 0.13$  eV (Planck Collaboration et al. 2018). Future improvements will likely continue to come from combining CMB data on large scales with clustering/lensing data on small scales and low redshifts, where the suppression of power by neutrinos is strongest (Brinckmann et al. 2019). But they will heavily rely on a better determination of  $\tau$ , the optical depth of reionization since CMB experiments measure the combined quantity  $A_s e^{-2\tau}$  (Allison et al. 2015; Liu et al. 2016; Archidiacono et al. 2017). Major upcoming CMB experiments, however, are ground-based (*e.g.* CMB-S4) and will not directly constrain  $\tau$  (Abazajian et al. 2016). Meanwhile, proposed future space-based experiments such as LiteBIRD<sup>1</sup> and LiteCORrE<sup>2</sup>, which have the greatest potential to precisely measure  $\tau$ , have yet to be confirmed.

Despite the  $\tau$  bottleneck in the near future, measuring the  $M_\nu$  imprint on the 3D clustering of galaxies provides a promising avenue for improving  $M_\nu$  constraints. With the unprecedented cosmic volumes they will probe, upcoming galaxy surveys such as DESI<sup>3</sup>, PFS<sup>4</sup>, EUCLID<sup>5</sup>, and WFIRST<sup>6</sup> have the potential to tightly constrain  $M_\nu$  (Audren et al. 2013; Font-Ribera et al. 2014; Petracca et al. 2016; Sartoris et al. 2016; Boyle & Komatsu 2018). Constraining  $M_\nu$  from 3D galaxy clustering, however, faces two limiting challenges: (1) accurate theoretical modeling beyond linear scales, for

<sup>1</sup> <http://litebird.jp/eng/>

<sup>2</sup> <http://www.core-mission.org/>

<sup>3</sup> <https://www.desi.lbl.gov/>

<sup>4</sup> <https://pfs.ipmu.jp/>

<sup>5</sup> <http://sci.esa.int/euclid/>

<sup>6</sup> <https://wfirst.gsfc.nasa.gov/>

bias tracers in redshift-space and (2) parameter degeneracies that limit the constraining power of standard two-point clustering analyses.

For the former, simulations have made huge strides in accurately modeling nonlinear structure formation with massive neutrinos (*e.g.* Brandbyge et al. 2008; Villaescusa-Navarro et al. 2013; Castorina et al. 2015; Adamek et al. 2017; Emberson et al. 2017; Banerjee et al. 2018; Villaescusa-Navarro et al. 2018, 2019). Moreover, new simulation-based approaches to modeling such as ‘emulation’ enable us to tractably exploit the accuracy of  $N$ -body simulations and analyze galaxy clustering on nonlinear scales beyond traditional perturbation theory methods. Recent works have applied these simulation-based approaches to analyze small-scale galaxy clustering with remarkable success (*e.g.* Heitmann et al. 2009; Kwan et al. 2015; Euclid Collaboration et al. 2018; Lange et al. 2019; Zhai et al. 2019; Wibking et al. 2019). These developments present the opportunity to significantly improve  $M_\nu$  constraints by unlocking the information content in nonlinear clustering, where the impact of massive neutrinos is strongest (*e.g.* Brandbyge et al. 2008; Saito et al. 2008; Wong 2008; Saito et al. 2009; Viel et al. 2010; Agarwal & Feldman 2011; Marulli et al. 2011; Bird et al. 2012; Castorina et al. 2015; Banerjee & Dalal 2016; Upadhye et al. 2016).

Villaescusa-Navarro et al. (2018) recently used more than 1000  $N$ -body simulations from the HADES suite to examine the redshift-space matter and halo power spectrum. They found that the imprint of  $M_\nu$  and  $\sigma_8$  on the redshift-space halo power spectrum are degenerate and differ by  $< 1\%$ . This  $M_\nu - \sigma_8$  degeneracy poses a serious limitation on constraining  $M_\nu$  with the power spectrum. However, information in the nonlinear regime cascades from the power spectrum to higher-order statistics such as the bispectrum. More importantly, these higher-order statistics help break the  $M_\nu - \sigma_8$  degeneracy (Hahn et al. 2020). Previous studies have already demonstrated the potential of the bispectrum for improving cosmological parameter constraints (Sefusatti & Scoccimarro 2005; Sefusatti et al. 2006; Chan & Blot 2017; Yankelevich & Porciani 2019). Chudaykin & Ivanov (2019), in particular, included  $M_\nu$  in their forecast and found that the bispectrum significantly improves constraints on  $M_\nu$ . However, none of these perturbation theory based forecast include the constraining power on nonlinear scales.

In Hahn et al. (2020), the previous paper of this series, we used 22,000  $N$ -body simulations from the QUIJOTE suite to quantify the total information content and constraining power of the redshift-space halo bispectrum down to nonlinear scales. For  $k_{\text{max}}=0.5 \ h/\text{Mpc}$ , we found that the bispectrum produces  $\Omega_m$ ,  $\Omega_b$ ,  $h$ ,  $n_s$ , and  $\sigma_8$  constraints 1.9, 2.6, 3.1, 3.6, and 2.6 times tighter than the power spectrum. For  $M_\nu$ , the bispectrum improved constraints by 5 times over the power spectrum. In this forecast, we marginalized over linear bias and halo mass limit parameters; we also found that the improvements on the constraints from the bispectrum are not impacted when we include quadratic and nonlocal bias parameters. Nevertheless, Hahn et al. (2020) focused on the halo bispectrum while actual constraints on  $M_\nu$  will be derived from the distribution of galaxies. Thus, a more realistic and complete galaxy bias model must be included.

In this work, we present the total information content and constraining power of the *redshift-space galaxy bispectrum* down to  $k_{\text{max}} = 0.5 \ h/\text{Mpc}$ . For our galaxy bias model, we use the halo occupation distribution (HOD) framework, which provides a statistical prescription for populating dark matter

halos with central and satellite galaxies. The HOD model has been successful in reproducing the observed galaxy clustering (*e.g.* Zheng et al. 2005; Leauthaud et al. 2012; Tinker et al. 2013; Zentner et al. 2016; Vakili & Hahn 2019). It is also the primary framework used in simulation-based clustering analyses (*e.g.* McClintock et al. 2018; Zhai et al. 2019; Lange et al. 2019; Wibking et al. 2019). We first construct 195,000 galaxy mock catalogs from the QUIJOTE  $N$ -body simulations then use them to calculate Fisher matrix forecasts. Afterwards, we present the constraining power of the galaxy bispectrum on  $M_\nu$  and other cosmological parameters after marginalizing over the HOD parameters. This work is the second paper in a series that aims to demonstrate the potential for simulation-based galaxy bispectrum analyses in constraining  $M_\nu$ . Later in the series, we will also present methods to tackle challenges that come with analyzing the full galaxy bispectrum, such as data compression to reduce its dimensionality. The series will culminate in fully simulation-based  $P_\ell^g$  and  $B_0^g$  reanalysis of SDSS-III BOSS.

In Sections 2 and 3, we describe the QUIJOTE  $N$ -body simulation suites and the HOD framework we use to construct galaxy mock catalogs from them. We then describe in Section 4, how we measure the bispectrum and calculate the Fisher forecasts of the cosmological parameters from the galaxy mocks. Finally, in Section 5, we present the full information content of the galaxy bispectrum and demonstrate how it significantly improves the constraints on the cosmological parameters:  $\Omega_m$ ,  $\Omega_b$ ,  $h$ ,  $n_s$ ,  $\sigma_8$ , and *especially*  $M_\nu$ .

## 2. THE QUIJOTE SIMULATION SUITE

For our forecasts we use simulations from the QUIJOTE suite, a set of over 43,000  $N$ -body simulations that spans over 7000 cosmological models and contains, at a single redshift, over 8.5 trillion particles (Villaescusa-Navarro et al. 2019). The QUIJOTE suite was designed to quantify the information content of cosmological observables and train machine learning algorithms. The suite includes enough realizations to accurately estimate covariance matrices of high-dimensional observables, such as the bispectrum, as well as the derivatives of these observables with respect to cosmological parameters. For the derivatives, the suite includes sets of simulations run at different cosmologies where only one parameter is varied from the fiducial cosmology:  $\Omega_m=0.3175$ ,  $\Omega_b=0.049$ ,  $h=0.6711$ ,  $n_s=0.9624$ ,  $\sigma_8=0.834$ , and  $M_\nu=0.0$  eV. Along  $\Omega_m$ ,  $\Omega_b$ ,  $h$ ,  $n_s$ , and  $\sigma_8$ , the fiducial cosmology is adjusted by either a step above or below the fiducial value:  $\{\Omega_m^+, \Omega_m^-, \Omega_b^+, \Omega_b^-, h^+, h^-, n_s^+, n_s^-, \sigma_8^+, \sigma_8^-\}$ . Along  $M_\nu$ , because  $M_\nu \geq 0.0$  eV and the derivative of certain observable with respect to  $M_\nu$  is noisy, QUIJOTE includes sets of simulations for  $\{M_\nu^+, M_\nu^{++}, M_\nu^{+++}\} = \{0.1, 0.2, 0.4 \text{ eV}\}$ . See Table 1 for a summary of the QUIJOTE simulations used in this work.

The initial conditions for all the simulations were generated at  $z=127$  using second-order perturbation theory for simulations with massless neutrinos ( $M_\nu = 0.0$  eV) and the Zel’dovich approximation for massive neutrinos ( $M_\nu > 0.0$  eV). The initial conditions with massive neutrinos take their scale-dependent growth factors/rates into account using the Zennaro et al. (2017) method, while for the massless neutrino case we use the traditional scale-independent rescaling. From the initial conditions, the simulations follow the gravitational evolution of  $512^3$  dark matter particles, and  $512^3$  neutrino particles for  $M_\nu > 0$  models, to  $z = 0$  using GADGET-III TreePM+SPH code (Springel 2005). Simulations with massive neutrinos are run using the “particle method”, where neutrinos are described

**Table 1.** The QUIJOTE suite includes 15,000 standard  $N$ -body simulations at the fiducial cosmology to accurately estimate the covariance matrices. It also includes sets of 500 simulations at 14 other cosmologies, where only one parameter is varied from the fiducial value (underlined), to estimate derivatives of observables along the cosmological parameters.

Name	$M_\nu$	$\Omega_m$	$\Omega_b$	$h$	$n_s$	$\sigma_8$	ICs	realizations
Fiducial	0.0	0.3175	0.049	0.6711	0.9624	0.834	2LPT	15,000
Fiducial ZA	0.0	0.3175	0.049	0.6711	0.9624	0.834	Zel’dovich	500
$M_\nu^+$	<u>0.1</u> eV	0.3175	0.049	0.6711	0.9624	0.834	Zel’dovich	500
$M_\nu^{++}$	<u>0.2</u> eV	0.3175	0.049	0.6711	0.9624	0.834	Zel’dovich	500
$M_\nu^{+++}$	<u>0.4</u> eV	0.3175	0.049	0.6711	0.9624	0.834	Zel’dovich	500
$\Omega_m^+$	0.0	<u>0.3275</u>	0.049	0.6711	0.9624	0.834	2LPT	500
$\Omega_m^-$	0.0	<u>0.3075</u>	0.049	0.6711	0.9624	0.834	2LPT	500
$\Omega_b^+$	0.0	0.3175	<u>0.051</u>	0.6711	0.9624	0.834	2LPT	500
$\Omega_b^-$	0.0	0.3175	<u>0.047</u>	0.6711	0.9624	0.834	2LPT	500
$h^+$	0.0	0.3175	0.049	<u>0.6911</u>	0.9624	0.834	2LPT	500
$h^-$	0.0	0.3175	0.049	<u>0.6511</u>	0.9624	0.834	2LPT	500
$n_s^+$	0.0	0.3175	0.049	0.6711	<u>0.9824</u>	0.834	2LPT	500
$n_s^-$	0.0	0.3175	0.049	0.6711	<u>0.9424</u>	0.834	2LPT	500
$\sigma_8^+$	0.0	0.3175	0.049	0.6711	0.9624	<u>0.849</u>	2LPT	500
$\sigma_8^-$	0.0	0.3175	0.049	0.6711	0.9624	<u>0.819</u>	2LPT	500

as a collisionless and pressureless fluid and therefore modeled as particles, same as CDM (Brandbyge et al. 2008; Viel et al. 2010). Halos are identified using the Friends-of-Friends algorithm (FoF; Davis et al. 1985) with linking length  $b = 0.2$  on the CDM + baryon distribution. We impose a halo mass limit of  $M_{\text{lim}} = 3.2 \times 10^{13} h^{-1} M_\odot$ . For the fiducial cosmology, the halo catalogs have  $\sim 156,000$  halos ( $\bar{n}_h \sim 1.56 \times 10^{-4} h^3 \text{Gpc}^{-3}$ ) with  $\bar{n}P_0(k = 0.1) \sim 3.23$ . We refer readers to Villaescusa-Navarro et al. (2019) and Hahn et al. (2020) for further details on the QUIJOTE simulations. The QUIJOTE simulations are publicly available at <https://github.com/franciscovillaescusa/Quijote-simulations>.

### 3. HALO OCCUPATION DISTRIBUTION

We are interested in quantifying the information content of the galaxy bispectrum. For a perturbation theory approach, this involves incorporating an analytic bias model for galaxies (*e.g.* Sefton et al. 2006; Yankelevich & Porciani 2019; Chudaykin & Ivanov 2019). Perturbation theory approaches, however, break down on small scales and cannot exploit the constraining power from nonlinear regime. Instead, in our simulation-based approach we use the halo occupation distribution (HOD) framework (*e.g.* Benson et al. 2000; Peacock & Smith 2000; Seljak 2000; Berlind & Weinberg 2002; Cooray & Sheth 2002; Zheng et al. 2005; Leauthaud et al. 2012; Tinker et al. 2013; Zentner et al. 2016; Vakili & Hahn 2019). HOD models statistically populate galaxies in dark matter halos

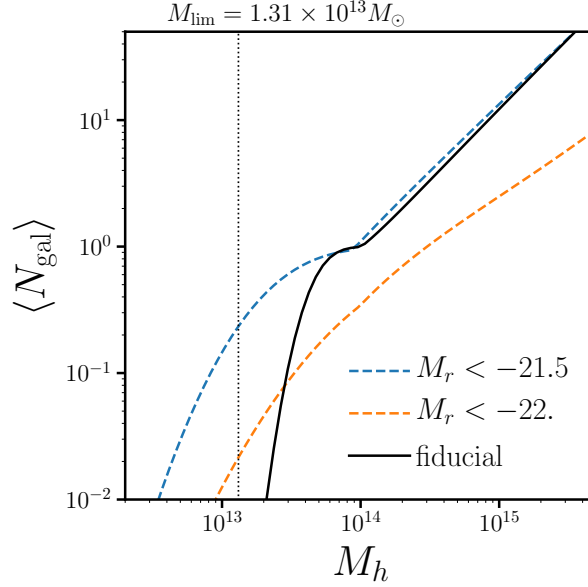


**Figure 1.** Our fiducial halo occupation (black) parameterized using the standard Zheng et al. (2007) HOD model. The parameter values of our fiducial HOD model (Eq. 4) are based on by the best-fit HOD parameters of the SDSS  $M_r < -21.5$  and  $< -22$ . samples from Zheng et al. (2007) modified to accommodate the  $M_{\text{lim}} = 3.2 \times 10^{13} h^{-1} M_{\odot}$  halo mass limit of the QUIJOTE simulations (black dotted). We include the best-fit halo occupations of the SDSS  $M_r < -21.5$  (blue dashed) and  $< -22$ . samples (orange dashed) from Zheng et al. (2007) for reference. Since our HOD parameters are based on the high luminosity SDSS samples, we do not include assembly bias. Our fiducial HOD galaxy catalog has a galaxy number density of  $\bar{n}_g \sim 1.63 \times 10^{-4} h^3/\text{Mpc}^3$  and linear bias of  $b_g \sim 2.55$ .

by specifying the probability of a given halo hosting a certain number of galaxies. This statistical prescription for connecting galaxies to halos has been remarkably successful in reproducing the observed galaxy clustering and, as a result, is the standard approach for constructing simulated galaxy mock catalogs in galaxy clustering analyses to estimate covariance matrices and test systematic effects (*e.g.* Rodríguez-Torres et al. 2016, 2017; Beutler et al. 2017). More importantly, HOD is the primary framework used in simulation-based galaxy clustering analyses: *e.g.* in emulation (McClintock et al. 2018; Zhai et al. 2019) or evidence modeling (Lange et al. 2019). Since the forecasts we present in this paper are aimed at quantifying the constraining power of the galaxy bispectrum for simulation-based analyses, the HOD model is particularly well-suited for our purpose.

In HOD models, the probability of a given halo hosting  $N$  galaxies of a certain class is dictated by its halo mass —  $P(N|M_h)$ . We use the standard HOD model from Zheng et al. (2007), which specifies the mean number of galaxies in a halo as

$$\langle N_{\text{gal}} \rangle = \langle N_{\text{cen}} \rangle + \langle N_{\text{sat}} \rangle \quad (1)$$

with mean central galaxy occupation

$$\langle N_{\text{cen}} \rangle = \frac{1}{2} \left[ 1 + \text{erf} \left( \frac{\log M_h - \log M_{\text{min}}}{\sigma_{\log M}} \right) \right] \quad (2)$$



and mean satellite galaxy occupation

$$\langle N_{\text{sat}} \rangle = \langle N_{\text{cen}} \rangle \left( \frac{M_h - M_0}{M_1} \right)^\alpha. \quad (3)$$

The mean number of centrals in a halo transitions smoothly from 0 to 1 for halos with mass  $M_h > M_{\text{min}}$ . The width of the transition is dictated by  $\sigma_{\log M}$ , which reflects the scatter between stellar mass/luminosity and halo mass. For  $M_h > M_{\text{min}}$ ,  $\langle N_{\text{sat}} \rangle$  follows a power law with slope  $\alpha$ .  $M_0$  is the halo mass cut-off for satellite occupation and  $M_h = M_0 + M_1$  is the typical mass scale for halos to host one satellite galaxy. The numbers of centrals and satellites for each halo are drawn from Bernoulli and Poisson distribution, respectively. Central galaxies are placed at the center of the halo while position and velocity of the satellite galaxies are sampled from a Navarro et al. (1997) (NFW) profile.

For the fiducial parameters of our HOD model we use values based on the best-fit HOD parameters for the SDSS  $M_r < -21.5$  and  $-22$  samples from Zheng et al. (2007):

$$\{M_{\text{min}}, \sigma_{\log M}, \log M_0, \alpha, \log M_1\} = \{13.65, 0.2, 14., 1.1, 14.\}. \quad (4)$$

In Figure 1, we present the halo occupation of our fiducial HOD parameters (black). We include the best-fit halo occupations of the SDSS  $M_r < -21.5$  (blue) and  $-22$  (orange) samples from Zheng et al. (2007) for comparison. We also mark the halo mass limit,  $M_{\text{lim}}$ , of the QUIJOTE simulations (black dotted). At  $M_h \sim 10^{13} M_\odot$ , the best-fit halo occupations of the SDSS samples extend below  $M_{\text{lim}}$  so halos below  $M_{\text{lim}}$  host galaxies. We therefore cannot use the exact best-fit HOD parameter values from the literature and instead reduce  $\sigma_{\log M}$  to 0.2 dex. The high  $\sigma_{\log M}$  in the  $M_r < -21.5$  and  $-22$  SDSS samples is caused by the turnover in the stellar-to-halo mass relation at high stellar masses (Mandelbaum et al. 2006; Conroy et al. 2007; More et al. 2011; Leauthaud et al. 2012; Tinker et al. 2013; Zu & Mandelbaum 2015; Hahn et al. 2019). Our fiducial halo occupation, with its lower  $\sigma_{\log M}$ , produces a galaxy sample with a tighter scatter between stellar mass/luminosity and  $M_h$  than the SDSS samples. In practice, constructing such a sample would require selecting based on observable galaxy properties that correlate more strongly with  $M_h$  than luminosity or  $M_*$ . While there is evidence that such observables are available (*e.g.*  $L_{\text{sat}}$ ; Alpaslan & Tinker 2019), they have not been adopted for selecting galaxy samples. Regardless, in this work our focus is on quantifying the information content of the galaxy bispectrum and not on analyzing a specific observed galaxy sample. We therefore opt for a more conservative set of HOD parameters with respect to  $M_{\text{lim}}$ , even if the resulting galaxy sample is less reflective of observations. For our fiducial halo occupation at the fiducial cosmology, the galaxy catalog has  $\bar{n}_g \sim 1.63 \times 10^{-4} h^3 \text{ Gpc}^{-3}$  and linear bias of  $b_g \sim 2.55$ .

The halo occupation in the Zheng et al. (2007) model depends solely on  $M_h$ . Simulations, however, find evidence that secondary halo properties such as concentration or formation history correlate with spatial distribution of halos — a phenomenon referred to as “halo assembly bias” (*e.g.* Sheth & Tormen 2004; Gao et al. 2005; Harker et al. 2006; Wechsler et al. 2006; Dalal et al. 2008; Wang et al. 2009; Lacerna et al. 2014; Contreras et al. 2020; Hadzhiyska et al. 2020). A model that only depends on  $M_h$ , does not account for this halo assembly bias and may not sufficiently describe

the connection between galaxies and halos. Moreover, if unaccounted for in the HOD model, and thus not marginalized over, halo assembly bias can impact the cosmological parameter constraints. However, for the high luminosity SDSS samples ( $M_r < -21.5$  and  $< -21$ ), [Zentner et al. \(2016\)](#) and [Vakili & Hahn \(2019\)](#) find little evidence for assembly bias in the galaxy clustering. Similarly, [Beltz-Mohrmann et al. \(2020\)](#) also find that the [Zheng et al. \(2007\)](#) HOD model is sufficient to reproduce galaxy clustering of luminous galaxies in hydrodynamic simulations. Since we base our HOD parameters on the high luminosity SDSS samples, we do not include assembly bias and use the [Zheng et al. \(2007\)](#) model.

All of the galaxy mock catalogs in this paper are constructed using the 22,000  $N$ -body simulations of the QUIJOTE suite: 15,000 at the fiducial cosmology and 500 at the 14 other cosmologies listed in Table 1. First, we construct mocks for estimating the covariance matrices using the 15,000 QUIJOTE sims at the fiducial cosmology with the fiducial HOD parameters. Next, we construct mocks for estimating the derivatives with respect to cosmological parameters using the 500 QUIJOTE sims at each of the 14 non-fiducial cosmologies. Finally, we construct mocks for estimating the derivatives with respect to the HOD parameters, using 500 QUIJOTE simulations at the fiducial cosmology with 10 sets of non-fiducial HOD parameters — a pair per parameter. Similar to the non-fiducial cosmologies in QUIJOTE, for each pair we vary one HOD parameter above and below the fiducial value by step sizes:

$$\{\Delta M_{\min}, \Delta \sigma_{\log M}, \Delta \log M_0, \Delta \alpha, \Delta \log M_1\} = \{0.05, 0.2, 0.2, 0.2, 0.2\}. \quad (5)$$

For the covariance matrix mocks, we generate one set of HOD realizations and apply RSD along the  $z$ -axis: 15,000 mocks. For the derivative mocks, we generate 5 sets of HOD realizations and apply RSD along all 3 directions: 180,000 mocks. *In total, we construct and use 195,000 galaxy catalogs in our analysis.* All of the galaxy catalogs are publicly available at [where to access the galaxy catalogs](#). TODO

#### 4. BISPECTRUM AND COSMOLOGICAL PARAMETER FORECASTS

We measure the bispectrum and calculate the parameter constraints using the same methods as [Hahn et al. \(2020\)](#). For further details, we refer readers to [Hahn et al. \(2020\)](#).

To measure  $B_0^g$ , we use a Fast Fourier Transform (FFT) based estimator similar to the ones described in [Sefusatti & Scoccimarro \(2005\)](#), [Scoccimarro \(2015\)](#), and [Sefusatti et al. \(2016\)](#). Galaxy positions are first interpolated onto a grid,  $\delta(\mathbf{x})$ , using a fourth-order interpolation scheme, which has advantageous anti-aliasing properties that allow unbiased measurements up to the Nyquist frequency ([Hockney & Eastwood 1981](#); [Sefusatti et al. 2016](#)). After Fourier transforming  $\delta(\mathbf{x})$  to get  $\delta(\mathbf{k})$ , we measure the bispectrum monopole:

$$B_0^g(k_1, k_2, k_3) = \frac{1}{V_B} \int_{k_1} d^3 q_1 \int_{k_2} d^3 q_2 \int_{k_3} d^3 q_3 \delta_D(\mathbf{q}_{123}) \delta(\mathbf{q}_1) \delta(\mathbf{q}_2) \delta(\mathbf{q}_3) - B_0^{\text{SN}}. \quad (6)$$

$\delta_D$  is the Dirac delta function,  $V_B$  is the normalization factor proportional to the number of triplets that can be found in the  $k_1, k_2, k_3$  triangle bin, and  $B_0^{\text{SN}}$  is the correction term for the Poisson shot noise. Throughout the paper, we use  $\delta(\mathbf{x})$  grids with  $N_{\text{grid}} = 360$  and triangle configurations defined by  $k_1, k_2, k_3$  bins of width  $\Delta k = 3k_f = 0.01885 h/\text{Mpc}$ , where  $k_f = 2\pi/(1000 h^{-1}\text{Mpc})$ .





**Figure 2.** The redshift-space galaxy power spectrum multipoles ( $P_\ell^g$ ; left) and bispectrum monopole ( $B_0^g$ ; right) of the fiducial HOD galaxy catalog (blue). The  $P_\ell^g$  and  $B_0^g$  are averaged over one set of HOD realizations run on 15,000  $N$ -body QUIJOTE simulations measured using the same FFT-based estimator as Hahn et al. (2020). In the left panel, we plot both the power spectrum monopole ( $\ell = 0$ ; solid) and quadrupole ( $\ell = 2$ ; dashed). In the right panel, we plot  $B_0^g$  for all 1898 triangle configurations with  $k_1, k_2, k_3 \geq k_{\max} = 0.5 h/\text{Mpc}$ . The configurations are ordered by looping through  $k_3$  in the inner most loop and  $k_1$  in the outer most loop satisfying  $k_1 \leq k_2 \leq k_3$ . We include for comparison the Hahn et al. (2020) halo  $P_\ell^h$  and  $B_0^h$  at the fiducial cosmology (black).

In Figure 2, we present the redshift-space galaxy power spectrum multipoles ( $P_\ell^g$ ; left) and bispectrum ( $B_0^g$ ; right) of the fiducial HOD galaxy catalog (blue). The  $P_\ell^g$  and  $B_0^g$  are averaged over one set of HOD realizations run on 15,000  $N$ -body QUIJOTE simulations at the fiducial cosmology. In the left panel, we plot both the power spectrum monopole ( $\ell = 0$ ; solid) and quadrupole ( $\ell = 2$ ; dashed). In the right panel, we plot  $B_0^g$  for all 1898 triangle configurations with  $k_1, k_2, k_3 \geq k_{\max} = 0.5 h/\text{Mpc}$ . The configurations are ordered by looping through  $k_3$  in the inner most loop and  $k_1$  in the outer most loop satisfying  $k_1 \leq k_2 \leq k_3$ . For comparison, we include the redshift-space halo power spectrum and bispectrum at the fiducial cosmology from Hahn et al. (2020) (black).

To estimate the constraining power of  $P_\ell^g$  and  $B_0^g$ , we use Fisher information matrices, which have been ubiquitously used in cosmology (*e.g.* Jungman et al. 1996; Tegmark et al. 1997; Dodelson 2003; Heavens 2009; Verde 2010):

$$F_{ij} = - \left\langle \frac{\partial^2 \ln \mathcal{L}}{\partial \theta_i \partial \theta_j} \right\rangle, \quad (7)$$

As in Hahn et al. (2020), we assume that the  $B_0^g$  likelihood is Gaussian and neglect the covariance derivative term (Carron 2013) and estimate the Fisher matrix as

$$F_{ij} = \frac{1}{2} \text{Tr} \left[ \mathbf{C}^{-1} \left( \frac{\partial B_0^g}{\partial \theta_i} \frac{\partial B_0^{gT}}{\partial \theta_j} + \frac{\partial B_0^{gT}}{\partial \theta_i} \frac{\partial B_0^g}{\partial \theta_j} \right) \right]. \quad (8)$$

We derive the covariance matrix,  $\mathbf{C}$ , using 15,000 fiducial galaxy catalogs. The derivatives along the cosmological and HOD parameters,  $\partial B_0^g / \partial \theta_i$ , are estimated using finite difference. For all parameters other than  $M_\nu$ , we estimate

$$\frac{\partial B_0^g}{\partial \theta_i} \approx \frac{B_0^g(\theta_i^+) - B_0^g(\theta_i^-)}{\theta_i^+ - \theta_i^-}, \quad (9)$$

where  $B_0^g(\theta_i^+)$  and  $B_0^g(\theta_i^-)$  are the average bispectrum of the 7,500 realizations at  $\theta_i^+$  and  $\theta_i^-$ , the HOD or cosmological parameter values above and below the fiducial parameters. For  $M_\nu$ , where the

**Table 2.** Marginalized Fisher parameter constraints from the redshift-space  $P_\ell$ ,  $B_0$ , and  $P_\ell + B_0$ . We list constraints for cosmological parameters  $M_\nu$ ,  $\Omega_m$ ,  $\Omega_b$ ,  $h$ ,  $n_s$ , and  $\sigma_8$  as well as HOD and nuisance parameters.

	$k_{\max} = 0.2$			$k_{\max} = 0.5$		
	$P_\ell$	$B_0$	$P_\ell + B_0$	$P_\ell$	$B_0$	$P_\ell + B_0$
$M_\nu$						
$\Omega_m$						
$\Omega_b$						
$h$						
$n_s$						
$\sigma_8$						
$M_{\min}$						
$\sigma_{\log M}$						
$\log M_0$						
$\alpha$						
$\log M_1$						

fiducial value is 0.0 eV, we use the galaxy catalogs at  $M_\nu^+$ ,  $M_\nu^{++}$ ,  $M_\nu^{+++} = 0.1, 0.2, 0.4$  eV (Table 1) to estimate

$$\frac{\partial B_0^g}{\partial M_\nu} \approx \frac{-21B_0^g(\theta_{\text{fid}}^{\text{ZA}}) + 32B_0^g(M_\nu^+) - 12B_0^g(M_\nu^{++}) + B_0^g(M_\nu^{+++})}{1.2}, \quad (10)$$

which provides a  $\mathcal{O}(\delta M_\nu^2)$  order approximation. Since the simulations at  $M_\nu^+$ ,  $M_\nu^{++}$ , and  $M_\nu^{+++}$  are generated from Zel'dovich initial conditions, we use simulations at the fiducial cosmology also generated from Zel'dovich initial conditions ( $\theta_{\text{fid}}^{\text{ZA}}$ ). Our simulation-based approach with galaxy catalogs constructed from  $N$ -body simulations is essential for accurately quantifying the constraining power of the bispectrum beyond the limitations of analytic methods down to nonlinear regimes.

## 5. RESULTS

We present the Fisher matrix constraints for  $M_\nu$  and other cosmological parameters from the redshift-space galaxy  $P_\ell^g$  (blue),  $B_0^g$  (green), and combined  $P_\ell^g + B_0^g$  (orange) in Figure 3. These constraints marginalize over the Zheng et al. (2007) HOD parameters (bottom panels) and extends to  $k_{\max} = 0.5 h/\text{Mpc}$ . The contours mark the 68% and 95% confidence intervals. With the redshift-space  $P_\ell^g$  alone, we derive the following  $1\sigma$  constraints for  $\{\Omega_m, \Omega_b, h, n_s, \sigma_8, M_\nu\}$ : **CH: 0.03443, 0.01219, 0.14069, 0.16552, 0.07701, 0.58119** With the redshift-space  $B_0^g$  alone, we get: **CH: 0.01422, 0.00371, 0.03409, 0.03543, 0.02494, 0.10599**. *The galaxy bispectrum substantially improves the constraints on all cosmological parameters over the power spectrum.*

With  $P_\ell^g$  and  $B_0^g$ , we derive even better constraints by breaking a number of parameter degeneracies. Among the cosmological parameters, the  $\Omega_m - \sigma_8$  degeneracy is broken and leads to significant improvements in both  $\Omega_m$  and  $\sigma_8$  constraints. Meanwhile, for the HOD parameters, degeneracies

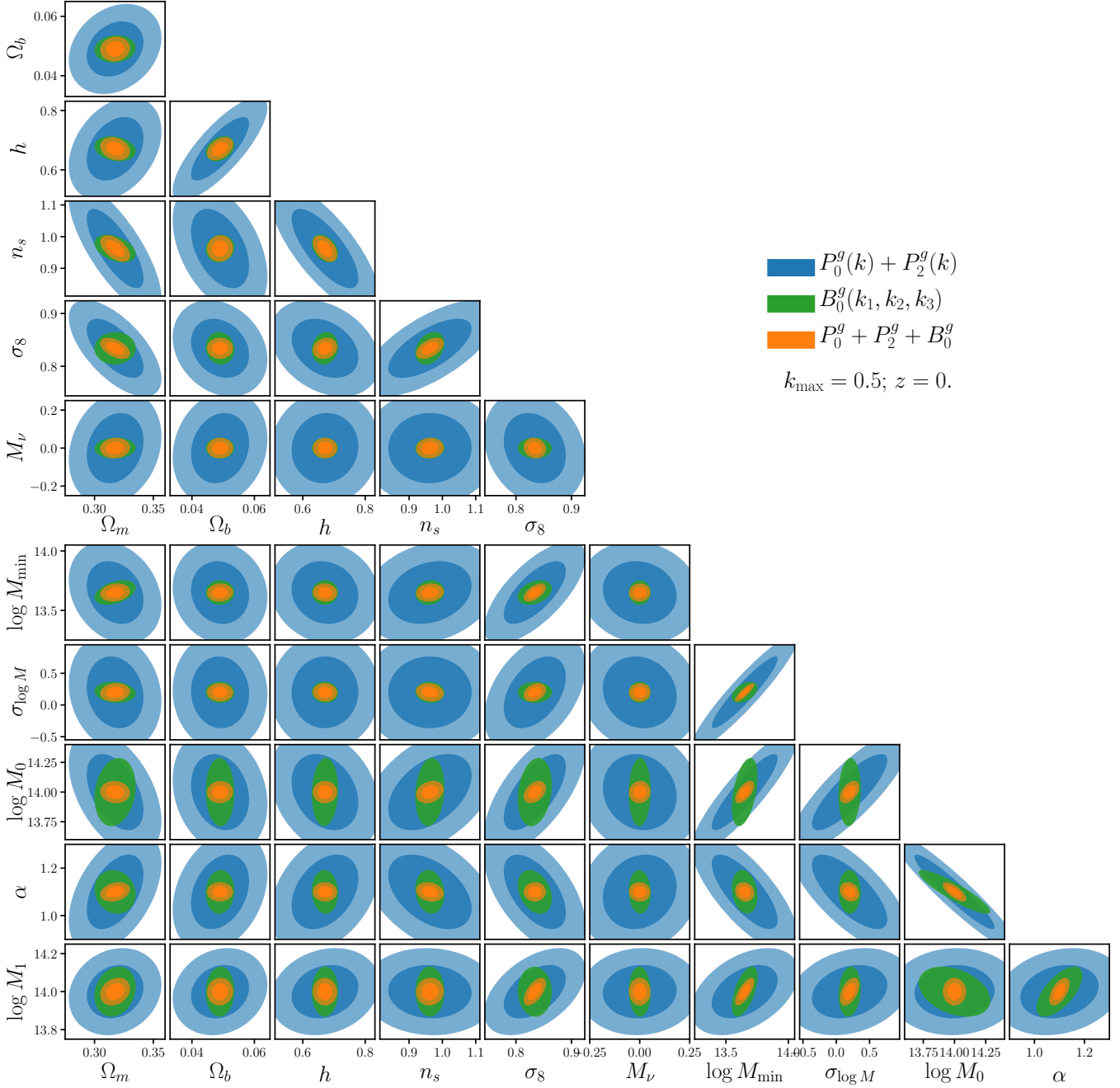


**Figure 3.** Fisher matrix constraints for  $M_\nu$  and other cosmological parameters for the redshift-space galaxy  $P_\ell^g$  (blue),  $B_0^g$  (green), and combined  $P_\ell^g$  and  $B_0^g$  (orange) for  $k_{\max} = 0.5 h/\text{Mpc}$ . Our forecasts marginalizes over the Zheng et al. (2007) HOD parameters:  $\{M_{\min}, \sigma_{\log M}, \log M_0, \alpha \log M_1\}$  (bottom panels). The contours mark the 68% and 95% confidence intervals. The bispectrum substantially improves constraints on all of the cosmological parameters over the power spectrum.  $\Omega_m$ ,  $\Omega_b$ ,  $h$ ,  $n_s$ , and  $\sigma_8$  constraints improve by factors of **CH: 1.9, 2.6, 3.1, 3.6, and 2.6**, respectively. For  $M_\nu$ , the bispectrum improves  $\sigma_{M_\nu}$  from **CH: 0.2968 to 0.0572 eV** — over a factor of  $\sim 5$  improvement over the power spectrum.

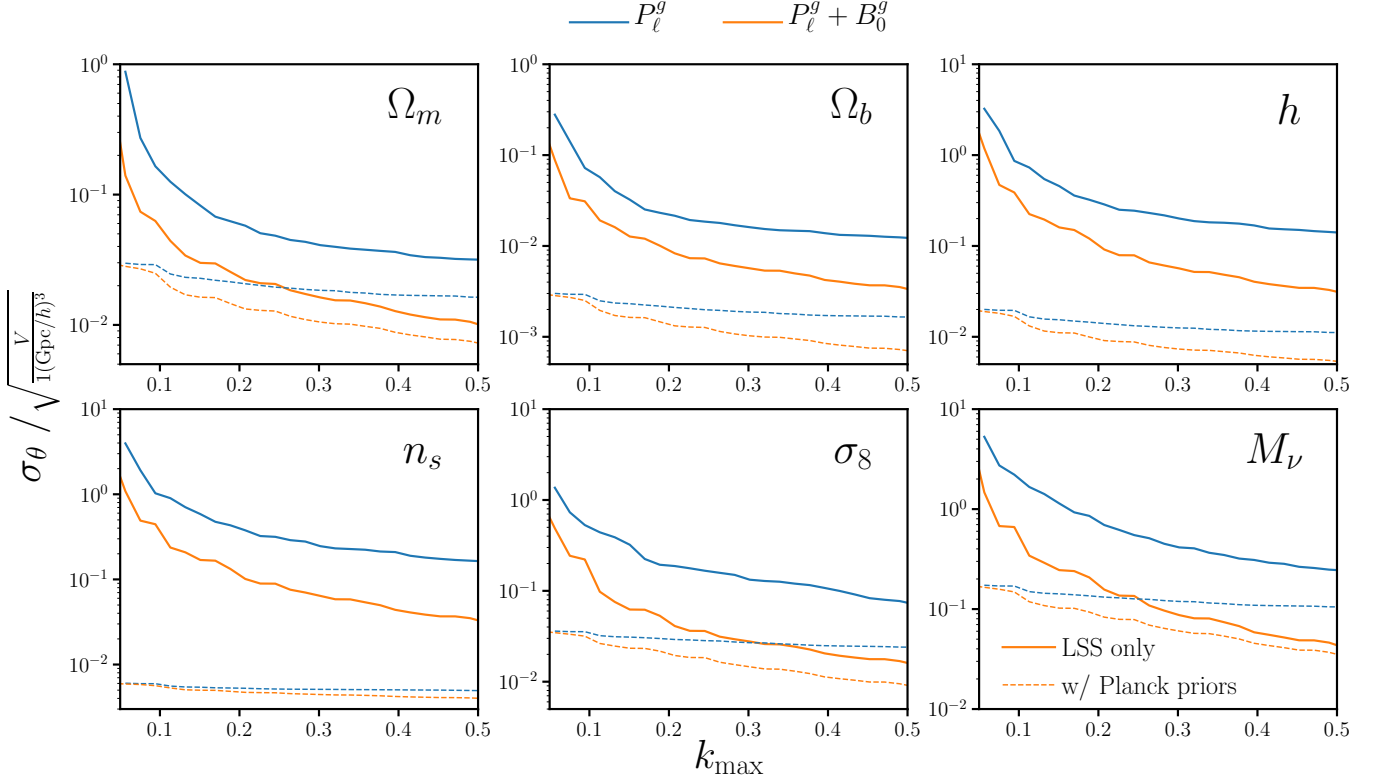


**Figure 4.** Marginalized  $1\sigma$  constraints,  $\sigma_\theta$ , of the cosmological parameters  $\Omega_m$ ,  $\Omega_b$ ,  $h$ ,  $n_s$ ,  $\sigma_8$ , and  $M_\nu$  as a function of  $k_{\max}$  for the redshift-space  $P_\ell^g$  (blue) and combined  $P_\ell^g + B_0^g$  (orange). Even after marginalizing over HOD parameters (Eq. 4), the galaxy bispectrum *significantly* improves cosmological parameter constraints above  $k_{\max} > 0.1 h/\text{Mpc}$ . Constraints from  $P_\ell^g$  and  $P_\ell^g + B_0^g$  improve with higher  $k_{\max}$ . Throughout  $0.2 < k_{\max} < 0.5$ , including the bispectrum improves  $\{\Omega_m, \Omega_b, h, n_s, \sigma_8, M_\nu\}$  by **CH: X, Y %**. When we include *Planck* priors (dotted), the improvement from  $B_0^g$  is even more evident. The constraining power of  $P_\ell^g$  complete saturates for  $k_{\max} \gtrsim 0.12 h/\text{Mpc}$ . Adding  $B_0^g$  not only improves constraints, but the constraints continue to improve for higher  $k_{\max}$ . At  $k_{\max} = 0.2$  and  $0.5 h/\text{Mpc}$ , the  $P_\ell^g + B_0^g$  improves the  $M_\nu$  constraint by **CH: X, Y %** over  $P_\ell^g$ . We emphasize that the constraints above are for  $1 (\text{Gpc}/h)^3$  box and thus underestimate the constraining power of upcoming galaxy clustering surveys.

with  $\log M_0$ ,  $\alpha$ , and  $\log M_1$  are substantially reduced. Combining  $P_\ell^g$  and  $B_0^g$ , we get the following  $1\sigma$  constraints for  $\Omega_m$ ,  $\Omega_b$ ,  $h$ ,  $n_s$ ,  $\sigma_8$ , and  $M_\nu$ : **CH: 0.01033, 0.00336, 0.03150, 0.03361, 0.01641, and 0.10299**. With  $P_\ell^g$  and  $B_0^g$  combined, we improve  $\Omega_m$ ,  $\Omega_b$ ,  $h$ ,  $n_s$ , and  $\sigma_8$  constraints by factors of **CH: 3.3, 3.6, 4.5, 4.9, and 4.7** and  $M_\nu$  constraint by a factor of 5.6.

In Figure 4, we present the marginalized  $1\sigma$  constraints,  $\sigma_\theta(k_{\max})$ , of the cosmological parameters  $\Omega_m$ ,  $\Omega_b$ ,  $h$ ,  $n_s$ ,  $\sigma_8$ , and  $M_\nu$  as a function of  $k_{\max}$  for  $P_\ell^g$  (blue) and the combined  $P_\ell^g + B_0^g$  (orange). Again, these constraints are marginalized over the Zheng et al. (2007) HOD parameters (Eq. 4). For both  $P_\ell^g$  and  $P_\ell^g + B_0^g$ , parameter constraints improve at higher  $k_{\max}$ . More importantly, *the galaxy bispectrum significantly improves constraints on all cosmological parameters throughout the*

$k_{\max}$  range and not only at high  $k_{\max}$ . Even for  $k_{\max} \sim 0.2 h/\text{Mpc}$ , including  $B_0^g$  improves  $\Omega_m$ ,  $\Omega_b$ ,  $h$ ,  $n_s$ ,  $\sigma_8$  and  $M_\nu$  constraints by factors of **CH: 2.6, 2.4, 2.7, 3.2, 4.1, and 3.6**.

We also present  $\sigma_\theta(k_{\max})$  for  $P_\ell^g$  (blue dashed) and  $P_\ell^g + B_0^g$  (orange dashed) *with priors from Planck*. Once we include *Planck* priors,  $P_\ell^g$  constraints do not improve for  $k_{\max} \gtrsim 0.12 h/\text{Mpc}$ . However, the constraining power of  $P_\ell^g + B_0^g$  continues to increase for  $k_{\max} > 0.15 h/\text{Mpc}$ . At  $k_{\max} = 0.2 h/\text{Mpc}$ ,  $B_0^g$  improves the  $P_\ell^g + \text{Planck}$  priors constraints on  $\Omega_m$ ,  $\Omega_b$ ,  $h$ ,  $n_s$ ,  $\sigma_8$  and  $M_\nu$  constraint by factors of **CH: 1.5, 1.4, 1.4, 1.1, 1.3, and 1.4 $\times$** . At  $k_{\max} = 0.5 h/\text{Mpc}$ ,  $B_0^g$  improves the  $P_\ell^g + \text{Planck}$  priors constraints on  $\Omega_m$ ,  $\Omega_b$ ,  $h$ ,  $n_s$ ,  $\sigma_8$  and  $M_\nu$  constraint by factors of **CH: 2.1, 2.1, 2.0, 1.2, 2.2, and 2.2 $\times$** . Even with *Planck* priors, the galaxy bispectrum significantly improves cosmological constraints. In fact, we emphasize that the constraints in Figure 4 are for a  $1 (\text{Gpc}/h)^3$  box. Hence, they *underestimate* the constraining power contribution from galaxy clustering that we expect from upcoming galaxy redshift surveys, which will probe a much larger volume (*e.g.* DESI, Euclid). With more constraining power coming from galaxy clustering, improvements from including  $B_0^g$  to  $P_\ell^g$  and *Planck* will be larger.

In the previous paper of the series, [Hahn et al. \(2020\)](#) presents the full information content of the redshift-space halo bispectrum,  $B_0^h$ . For  $B_0^h$  to  $k_{\max} = 0.5 h/\text{Mpc}$ , [Hahn et al. \(2020\)](#) find  $1\sigma$  constraints of 0.012, 0.004, 0.04, 0.036, 0.014, and 0.057 for  $\Omega_m$ ,  $\Omega_b$ ,  $h$ ,  $n_s$ ,  $\sigma_8$  and  $M_\nu$ . In comparison, we find that  $B_0^g$  produces comparable constraints for  $\Omega_b$ ,  $h$ , and  $n_s$ . On the other hand,  $B_0^g$  has less constraining power than  $B_0^h$  for  $\Omega_m$ ,  $\sigma_8$ , and  $M_\nu$ . This is the same for  $k_{\max} = 0.2 h/\text{Mpc}$ . When we compare the signal-to-noise ratios (SNR) of  $B_0^g$  and  $B_0^h$ , estimated from the covariance matrix (*e.g.* [Sefusatti & Scoccimarro 2005](#); [Sefusatti et al. 2006](#); [Chan & Blot 2017](#)), we find lower SNR for  $B_0^g$ , consistent with the constraints. We also find that the increase in SNR with  $k_{\max}$  is lessened for  $B_0^g$ . This demonstrates that marginalizing over HOD parameters reduces some of the constraining power of  $B_0^g$ . Fingers-of-god (FoG), also contributes to this reduction. **CH: elaborate on how FoG.** Nevertheless,  $B_0^g$  significantly improves parameters constraints over  $P_\ell^g$ . In fact, marginalizing over HOD parameters and FoG reduces the constraining power of the power spectrum more so than the bispectrum. Therefore, we find larger improvements in the parameter constraints from  $B_0^g$  over  $P_\ell^g$  than from  $B_0^h$  over  $P_\ell^h$ .

A number of previous works have quantified the information content of the bispectrum: (*e.g.* [Scoccimarro et al. 2004](#); [Sefusatti et al. 2006](#); [Sefusatti & Komatsu 2007](#); [Song et al. 2015](#); [Tellarini et al. 2016](#); [Yamauchi et al. 2017](#); [Karagiannis et al. 2018](#); [Yankelevich & Porciani 2019](#); [Chudaykin & Ivanov 2019](#); [Coulton et al. 2019](#); [Reischke et al. 2019](#)). We, however, focus our comparison to [Sefusatti et al. \(2006\)](#), [Yankelevich & Porciani \(2019\)](#), and [Chudaykin & Ivanov \(2019\)](#), which provide bispectrum forecasts for full sets of cosmological parameters. [Sefusatti et al. \(2006\)](#) present  $\Lambda\text{CDM}$  forecasts for a joint likelihood analysis of  $B_0^g$  with  $P^g$  and WMAP. For  $k_{\max} = 0.2 h/\text{Mpc}$ , they find that including  $B_0^g$  improves constraints on  $\Omega_m$ ,  $\Omega_b$ ,  $h$ ,  $n_s$ , and  $\sigma_8$  by 1.6, 1.2, 1.5, 1.4, and 1.5 times from the  $P^g$  and WMAP constraints. In comparison, for  $k_{\max} = 0.2 h/\text{Mpc}$  and with *Planck* priors, we find  $B_0^g$  improves constraints by 1.5, 1.4, 1.4, 1.1, and 1.3 $\times$ , which is in good agreement with [Sefusatti et al. \(2006\)](#). We note, however, that there are some significant differences in our analyses. First, [Sefusatti et al. \(2006\)](#) uses the WMAP likelihood while we use priors from

*Planck*. Furthermore, in our simulation-based approach, we marginalize over the HOD parameters. On the other hand, Sefusatti et al. (2006) use a perturbation theory approach and marginalize over the linear and quadratic bias terms ( $b_1, b_2$ ). Nevertheless, the improvement Sefusatti et al. (2006) find in parameter constraints including  $B_0^g$  is in good agreement with our results.

Next, Yankelevich & Porciani (2019) present  $\Lambda$ CDM,  $w$ CDM and  $w_0w_a$ CDM Fisher forecasts for a Euclid-like survey? over  $0.65 < z < 2.05$ . Focusing only on their  $\Lambda$ CDM forecasts, they find that for  $k_{\max} = 0.15 h/\text{Mpc}$ ,  $P^g + B_0^g$  produces constraints on  $\Omega_{\text{cdm}}, \Omega_b, A_s, h, n_s$  that are  $\sim 1.3\times$  tighter than  $P^g$  alone. With *Planck* priors, they find parameter constraints improve by a factor of  $\sim 1.1$ . In contrast, we find even at  $k_{\max} = 0.15 h/\text{Mpc}$  significantly larger improvement in the parameter constraints from including  $B_0^g$ . However, we similarly find that the improvement decreases once we include *Planck* priors (Figure 4).

Although Yankelevich & Porciani (2019) find significantly less improvement in parameter constraints from  $B_0^g$ , we emphasize that Yankelevich & Porciani (2019) present forecasts for a significantly different galaxy sample — *i.e.* the Euclid survey over  $0.65 < z < 2.05$ . For instance, their  $z = 0.7$  redshift bin has  $\bar{n}_g = 2.76 \times 10^{-3} h^3\text{Gpc}^{-3}$  and linear bias of  $b_g = 1.18$ . Meanwhile our galaxy sample is at  $z = 0$  with  $\bar{n}_g \sim 1.63 \times 10^{-4} h^3\text{Gpc}^{-3}$  and linear bias of  $b_g \sim 2.55$  (Section 3). Furthermore, while we use the HOD framework, they use a bias expansion with linear, non-linear, and tidal bias ( $b_1, b_2$ , and  $b_{s^2}$ ). They also marginalize over 56 nuisance parameters since they jointly analyze 14  $z$  bins, each with 4 nuisance parameters. Lastly, unlike our simulation-based approach, Yankelevich & Porciani (2019) use perturbation theory models and, therefore, limit their forecast to  $k_{\max} = 0.15 h/\text{Mpc}$  due to theoretical uncertainties. Nevertheless, when they estimate the constraining power beyond  $k_{\max} > 0.15 h/\text{Mpc}$  using Figure of Merit they find that the constraining power of  $B_0^g$  relative to  $P^g$  increases for higher  $k_{\max}$  consistent with our results.

Finally, Chudaykin & Ivanov (2019) present  $M_\nu + \Lambda$ CDM forecasts for the power spectrum and bispectrum of a Euclid-like survey over  $0.5 < z < 2.1$ . For  $\omega_{\text{cdm}}, \omega_b, h, n_s, A_s$ , and  $M_\nu$  they find  $\sim 1.2, 1.5, 1.4, 1.3$ , and  $1.1\times$  tighter constraints from  $P_\ell^g$  and  $B_0^g$  than from  $P_\ell^g$  alone. For  $M_\nu$ , they find a factor of 1.4 improvement, from 0.038 eV to 0.028 eV. With *Planck*, they get  $\sim 2, 1.1, 2.3, 1.5, 1.1$ , and  $1.3\times$  tighter constraints for  $\omega_{\text{cdm}}, \omega_b, h, n_s, A_s$ , and  $M_\nu$  from including  $B_0^g$ . Overall, Chudaykin & Ivanov (2019) find significant improvements from including  $B_0^g$  — consistent with our results. However, they find more modest improvements than we find in Figures 3 and 4.

Again, there are significant differences between our analyses. First, like Yankelevich & Porciani (2019), Chudaykin & Ivanov (2019) present forecasts for a Euclid-like survey, which is significantly different than our galaxy sample. Their  $z = 0.6$  redshift bin, for instance, has  $\bar{n}_g = 3.83 \times 10^{-3} h^3\text{Gpc}^{-3}$  and linear bias of  $b_g = 1.14$ . Next, they include the Alcock-Paczynski (AP) effect for  $P_\ell^g$  but not for  $B_0^g$ . They find that including the AP effect significantly improves  $P_\ell^g$  constraints (e.g. tightens  $M_\nu$  constraints by  $\sim 30\%$ ); this reduces the improvement they report from including  $B_0^g$ .

Another difference between our analyses is that although Chudaykin & Ivanov (2019) use a more accurate Markov-Chain Monte-Carlo (MCMC) approach to derive parameter constraints, they neglect the non-Gaussian contributions to both  $P_\ell^g$  and  $B_0^g$  covariance matrices and also do not include the covariance between  $P_\ell^g$  and  $B_0^g$  for the joint constraints. We find that neglecting the covariance



between  $P_\ell^g$  and  $B_0^g$  overestimates constraints by **CH: XXXX** for our  $k_{\max} = 0.2 h/\text{Mpc}$  constraints. Lastly, Chudaykin & Ivanov (2019) use a one-loop and tree-level perturbation theory to model  $P_\ell^g$  and  $B_0^g$ , respectively. Rather than imposing a  $k_{\max}$  cutoff to restrict their forecasts to scales where their perturbation theory models can be trusted, they use a theoretical error covariance model approach from ?. With a tree-level  $B_0^g$  model, theoretical errors quickly dominate at  $k_{\max} \gtrsim 0.1 h/\text{Mpc}$ , where one- and two-loop contribute significantly (*e.g.* Lazanu & Liguori 2018). So effectively, their forecasts do not include the constraining power on those scales. In fact, if we restrict our forecast to  $k_{\max} = 0.25 h/\text{Mpc}$  for  $P_\ell^g$  and  $k_{\max} = 0.1 h/\text{Mpc}$  for  $B_0^g$ , our  $\Omega_m$ ,  $\Omega_b$ ,  $h$ ,  $n_s$ ,  $\sigma_8$ , and  $M_\nu$  constraints improve by 1.3, 1.2, 1.2, 1.4, 2.0, and  $1.7\times$  from including  $B_0^g$ , roughly consistent with Chudaykin & Ivanov (2019).

Among the various differences between our forecast and previous works, we emphasize that we use a simulation-based approach. This, combined with the immense number of simulations, is what allows us to go beyond previous perturbation theory approaches and accurately quantify the constraining power in the nonlinear regime. Furthermore, this allows us to derive, for the first time, the total information content of the redshift-space galaxy power spectrum and bispectrum down to nonlinear scales and demonstrate the constraining power of the galaxy bispectrum for  $M_\nu$ .

A simulation-based approach, however, has a few caveats, which we discuss below. First, our forecasts rely on the stability and convergence of the covariance matrix and numerical derivatives. For our constraints we use 195000 galaxy catalogs (Section 3): 15,000 for the covariance matrices and 180,000 for the derivatives with respect to 11 parameters. To ensure that our results are robust, we conduct the same set of convergence tests as Hahn et al. (2020). First, we test whether our results have sufficiently converged by deriving our constraints using different numbers of galaxy catalogs to estimate the covariance matrix and derivatives:  $N_{\text{cov}}$  and  $N_{\text{deriv}}$ . For  $N_{\text{cov}}$ , we find  $< XXXX\%$  variation  $\sigma_\theta$  for  $N_{\text{cov}} > 12000$ . For  $N_{\text{deriv}}$ , we find  $< XXXX\%$  variation  $\sigma_\theta$  for  $N_{\text{cov}} > 12000$ . vary by  $< 10\%$ , we conclude that the convergence of the covariance matrix or derivatives do not significantly impact our forecast. **CH: fill this in once we have the convergence test.**

Besides the convergence of the numerical derivatives, the  $M_\nu$  derivatives can be evaluated using different sets of cosmologies. In our analysis, we evaluate  $\partial P_\ell^g / \partial M_\nu$  and  $\partial B_0^g / \partial M_\nu$  using simulations at the  $\{\theta_{\text{ZA}}, M_\nu^+, M_\nu^{++}, M_\nu^{+++}\}$  cosmologies. They can, however, also be estimated using two other sets of cosmologies: (i)  $\{\theta_{\text{ZA}}, M_\nu^+\}$  and (ii)  $\{\theta_{\text{ZA}}, M_\nu^+, M_\nu^{++}\}$ . If we used (i) estimates for  $\partial P_\ell^g / \partial M_\nu$  and  $\partial B_0^g / \partial M_\nu$ , compared to our forecasts, we get **CH: XXXXX**. For (ii), we get **CH: XXXX**. **CH: check this once the multiple HOD seeds finish.**

For our fiducial HOD parameters other than  $\sigma_{\log M}$ , we chose values based on Zheng et al. (2007) fits to the SDSS  $M_r < -21.5$  and  $-22$  samples (Section 3). For  $\sigma_{\log M}$ , due to the halo mass limit of QUIJOTE, we chose a tighter scatter of 0.2 dex. As a result, our HOD galaxy catalogs have a different selection function than observed samples, which are typically based on  $M_r$  or  $M_*$  cuts (*e.g.* SDSS or BOSS). To test the impact of the fiducial  $\sigma_{\log M}$  choice, **CH: in Appendix ??, we compare  $\partial P_\ell^g / \partial \sigma_{\log M}$  and  $\partial B_0^g / \partial \sigma_{\log M}$  at  $\sigma_{\log M} = 0.2$  dex to the derivatives evaluated at  $\sigma_{\log M} =$ , estimated using higher resolution QUIJOTE simulations. Fill in after we do the comparison. CH: what can we say about the sigma8-sigma logM degeneracy?**

Besides their convergence and stability, our forecasts are derived from Fisher matrices. We, therefore, assume that the posterior is approximately Gaussian. When posteriors are highly non-elliptical or asymmetric, Fisher forecasts significantly underestimate the constraints (Wolz et al. 2012). We note that in this paper we do not derive actual parameter constraints. Instead, we focus on quantifying the information content and constraining power of  $B_0^g$  relative to  $P_\ell^g$ . Hence, we do not explore beyond the Fisher forecast. In a later paper of the series, when we analyze the SDSS-III BOSS data using a simulation-based approach, we will use a robust method to sample the posterior.

Besides the caveats above, a number of extra steps and complications remain between this work and a full galaxy bispectrum analysis using a simulation based approach. For instance, we use the basic Zheng et al. (2007) HOD model, which does not include assembly bias. Zentner et al. (2016) and Vakili & Hahn (2019) find little evidence for assembly bias in the galaxy clustering of the SDSS  $M_r < -21.5$  and  $-21$  samples. Beltz-Mohrmann et al. (2020) also found that the basic HOD is sufficient to reproduce several galaxy clustering statistics (*e.g.* projected 2PCF, 2PCF, group multiplicity function) of high luminosity galaxies in the Illustris and EAGLE hydrodynamic simulations. While the basic HOD is likely sufficient for the forecast we present, many works have demonstrated that assembly bias impacts galaxy clustering for lower luminosity/mass samples both using observations (Vakili & Hahn 2019; ?) and hydrodynamic simulations (Chaves-Montero et al. 2016; Beltz-Mohrmann et al. 2020).

In addition to assembly bias, central and satellite velocity biases can also impact galaxy clustering (Guo et al. 2015b,a). Central galaxies, in both observations and simulations, are not at rest in the centers of the host halos (*e.g.* ????). Similarly, satellite galaxies in simulations do not have the same velocities as the underlying dark matter (*e.g.* ??????). This velocity bias in centrals reduces the Kaiser effect; while in satellites, it reduces the FoG effect. For the high luminosity SDSS samples, Guo et al. (2015a) find little satellite velocity bias. While they find some central velocity bias, their constraints are based on galaxy clustering on very small scales ( $\sim 0.1 - 25 h^{-1} \text{Mpc}$ ). More recently, ? found that removing central and satellite velocity biases for the Illustris and EAGLE simulations had little impact on various clustering measurements of their high luminosity sample. Although assembly bias and velocity bias do not likely impact the forecasts we present, for lower luminosity/mass galaxy samples and for higher precision measurements of observations they must be included. The improvements we see in HOD parameter constraints from  $B_0^g$  in Figure 3 suggest that  $B_0^g$  also has the potential to better constrain the assembly bias parameters and improve our understanding of the galaxy-halo connection. Therefore, when we analyze observations with a simulation-based approach later in the series, we will use a decorated HOD framework (such as *e.g.* Vakili & Hahn 2019; Zhai et al. 2019, CH: others) that includes both assembly bias and velocity biases.

Our analysis also does not include baryonic effects. Although they have been typically neglected in galaxy clustering analyses, baryonic effects, such as feedback from active galactic nuclei (AGN), can impact the matter distribution at cosmological distances (*e.g.* Harnois-Déraps et al. 2015). For AGN feedback in particular, various works have an impact on the matter power spectrum (*e.g.* van Daalen et al. 2020). Although there is no consensus on the magnitude of the effect, ultimately, a more effective AGN feedback increases the impact on the matter clustering (Barreira et al.

2019). In state-of-the-art hydrodynamical simulations (TNG, EAGLE, and BAHAMAS), Foreman et al. (2019) find  $\lesssim 1\%$  impact on the matter power spectrum at  $k \lesssim 0.5 h/\text{Mpc}$ . For the matter bispectrum, Foreman et al. (2019) find that the effect of baryons is peaked at  $k = 3 h/\text{Mpc}$  and, similarly, a  $\lesssim 1\%$  effect at  $k \lesssim 0.5 h/\text{Mpc}$ . Despite the growing evidence of baryon impacting the matter clustering, the effect is mainly seen on scales smaller than what is probed by galaxy clustering analyses with spectroscopic redshift surveys. We, therefore, do not include baryonic effects in our forecasts and do not consider it further in the series.

In our forecasts, we use  $B_0^g$  with triangle defined in  $k_1, k_2, k_3$  bins of width  $\Delta k = 3k_f = 0.01885 h/\text{Mpc}$  (Section 4). Gagrani & Samushia (2017) find that for the growth rate parameter bispectrum multipoles beyond the monopole have significant constraining power. Yankelevich & Porciani (2019), with figure-of-merit (FoM) estimates, also find significant information content beyond the monopole. Furthermore, Yankelevich & Porciani (2019) also find that coarser binning of the triangle configurations reduces the information content of the bispectrum. Binning by  $\Delta k = 3k_f$  has  $\sim 10\%$  less constraining power than binning by  $\Delta k = k_f$ . Including higher order multipoles and increase the binning are both straightforward to implement; however, they both increase the dimensionality of the data vector.  $B_0^g$  alone binned by  $\Delta k = 3k_f$  already has 1898 dimensions. Hence, including multipoles and increasing the binning is not feasible for a full bispectrum analysis without the use of data compression (*e.g.* Byun et al. 2017; Gualdi et al. 2018, 2019b,a). For future papers in the series, we will include bispectrum multipoles and finer binning in conjunction with data compression.

Lastly, our forecasts are derived using periodic boxes and do not consider a realistic geometry or radial selection function of galaxy surveys. A realistic selection function will smooth the triangle configuration dependence and degrade the constraining power of the bispectrum (Sefusatti & Scoccimarro 2005). We also do not account for super-sample covariance, which may also impact our constraints (Hamilton et al. 2006; Sefusatti et al. 2006; Takada & Hu 2013; Li et al. 2018; Wadekar & Scoccimarro 2019). Since these effects also affect the power spectrum, we expect to find substantial improvements in cosmological parameter constraints from including the bispectrum, especially for  $M_\nu$ .

In this paper, we present the total information content and constraining power of the galaxy bispectrum down to the nonlinear regime. Even after marginalizing over galaxy bias, through the HOD parameters, including  $B_0^g$  provides substantial improvements in cosmological parameter constraints — especially  $M_\nu$ . A combined analysis of  $P_\ell^g$  and  $B_0^g$  breaks several key parameter degeneracies that limit an analysis of  $P_\ell^g$  alone. We find that the significant improvements from  $B_0^g$  even at  $k_{\text{max}} \sim 0.2 h/\text{Mpc}$  and with *Planck* priors. Furthermore, we emphasize that the constraints we present is for a  $1 h^{-1}\text{Gpc}$  box and  $\bar{n}_g \sim 1.63 \times 10^{-4} h^3\text{Gpc}^{-3}$ . Upcoming surveys will probe substantially larger cosmic volumes with higher number densities. We discuss a number of factors that will impact the constraining power of  $B_0^g$  for actual galaxy clustering analyses, such as assembly bias, survey geometry, super-sample covariance, and etc. Even if the constraining power is reduced, our forecasts suggest that the galaxy bispectrum will significantly improve cosmology parameter constraints.

Now that we have demonstrated the constraining power of  $B_0^g$ , in the following paper of this series we will address a major practical challenge for a  $B_0^g$  analysis — its large dimensionality. We will

present how data compression can be used to reduce the dimensionality and tractably estimate the covariance matrix in a  $P_\ell^g$  and  $B_0^g$  analysis using a simulation-based approach. Afterwards, the series will culminate in fully simulation-based  $P_\ell^g$  and  $B_0^g$  reanalysis of SDSS-III BOSS.

## 6. SUMMARY

Afterwards, we will apply it to future surveys. **CH: rough numbers of DESI, PFS, and Euclid**

## ACKNOWLEDGEMENTS

It's a pleasure to thank Mehmet Alpaslan, Arka Banerjee, Joseph DeRose, Daniel Eisenstein, Mikhail Ivanov, Elena Massara, Jeremy L. Tinker, Roman Scoccimarro, Uroš Seljak, Zachary Slepian, Digvijay Wadekar, Risa Wechsler ... for valuable discussions and comments.

## APPENDIX

## REFERENCES

- Abazajian, K. N., Adshead, P., Ahmed, Z., et al. 2016, [arXiv:1610.02743 \[astro-ph, physics:gr-qc, physics:hep-ph, physics:hep-th\]](#), [arXiv:1610.02743 \[astro-ph, physics:gr-qc, physics:hep-ph, physics:hep-th\]](#)
- Adamek, J., Durrer, R., & Kunz, M. 2017, [arXiv:1707.06938 \[astro-ph, physics:gr-qc\]](#), [arXiv:1707.06938 \[astro-ph, physics:gr-qc\]](#)
- Agarwal, S., & Feldman, H. A. 2011, [Monthly Notices of the Royal Astronomical Society](#), 410, 1647
- Allison, R., Caucal, P., Calabrese, E., Dunkley, J., & Louis, T. 2015, [Physical Review D](#), 92, 123535
- Alpaslan, M., & Tinker, J. L. 2019, [arXiv e-prints](#), 1911, [arXiv:1911.04509](#)
- Archidiacono, M., Brinckmann, T., Lesgourgues, J., & Poulin, V. 2017, [Journal of Cosmology and Astro-Particle Physics](#), 2017, 052
- Audren, B., Lesgourgues, J., Bird, S., Haehnelt, M. G., & Viel, M. 2013, [Journal of Cosmology and Astro-Particle Physics](#), 2013, 026
- Banerjee, A., & Dalal, N. 2016, [Journal of Cosmology and Astro-Particle Physics](#), 2016, 015
- Banerjee, A., Powell, D., Abel, T., & Villaescusa-Navarro, F. 2018, [arXiv:1801.03906 \[astro-ph\]](#), [arXiv:1801.03906 \[astro-ph\]](#)
- Barreira, A., Nelson, D., Pillepich, A., et al. 2019, [Monthly Notices of the Royal Astronomical Society](#), 488, 2079
- Beltz-Mohrmann, G. D., Berlind, A. A., & Szewciw, A. O. 2020, [Monthly Notices of the Royal Astronomical Society](#), 491, 5771
- Benson, A. J., Cole, S., Frenk, C. S., Baugh, C. M., & Lacey, C. G. 2000, [Monthly Notices of the Royal Astronomical Society](#), 311, 793
- Berlind, A. A., & Weinberg, D. H. 2002, [The Astrophysical Journal](#), 575, 587
- Beutler, F., Seo, H.-J., Saito, S., et al. 2017, [Monthly Notices of the Royal Astronomical Society](#), 466, 2242
- Bird, S., Viel, M., & Haehnelt, M. G. 2012, [Monthly Notices of the Royal Astronomical Society](#), 420, 2551
- Bonn, J., Eitel, K., Glück, F., et al. 2011, [Physics Letters B](#), 703, 310
- Boyle, A., & Komatsu, E. 2018, [Journal of Cosmology and Astro-Particle Physics](#), 2018, 035
- Brandbyge, J., Hannestad, S., Haugbølle, T., & Thomsen, B. 2008, [Journal of Cosmology and Astro-Particle Physics](#), 08, 020
- Brinckmann, T., Hooper, D. C., Archidiacono, M., Lesgourgues, J., & Sprenger, T. 2019, [Journal of Cosmology and Astroparticle Physics](#), 2019, 059
- Byun, J., Eggemeier, A., Regan, D., Seery, D., & Smith, R. E. 2017, [Monthly Notices of the Royal Astronomical Society](#), 471, 1581
- Carron, J. 2013, [Astronomy & Astrophysics](#), 551, A88

- Castorina, E., Carbone, C., Bel, J., Sefusatti, E., & Dolag, K. 2015, *Journal of Cosmology and Astro-Particle Physics*, 2015, 043
- Chan, K. C., & Blot, L. 2017, *Physical Review D*, 96, [arXiv:1610.06585](#)
- Chaves-Montero, J., Angulo, R. E., Schaye, J., et al. 2016, *Monthly Notices of the Royal Astronomical Society*, 460, 3100
- Chudaykin, A., & Ivanov, M. M. 2019, [arXiv:1907.06666 \[astro-ph, physics:hep-ph\]](#), [arXiv:1907.06666 \[astro-ph, physics:hep-ph\]](#)
- Conroy, C., Prada, F., Newman, J. A., et al. 2007, *The Astrophysical Journal*, 654, 153
- Contreras, S., Angulo, R., & Zennaro, M. 2020, *arXiv e-prints*, 2005, [arXiv:2005.03672](#)
- Cooray, A., & Sheth, R. 2002, *Physics Reports*, 372, 1
- Coulton, W. R., Liu, J., Madhavacheril, M. S., Böhm, V., & Spergel, D. N. 2019, *Journal of Cosmology and Astro-Particle Physics*, 2019, 043
- Dalal, N., Doré, O., Huterer, D., & Shirokov, A. 2008, *Physical Review D*, 77, [arXiv:0710.4560](#)
- Davis, M., Efstathiou, G., Frenk, C. S., & White, S. D. M. 1985, *The Astrophysical Journal*, 292, 371
- Dodelson, S. 2003, *Modern Cosmology*
- Drexlin, G., Hannen, V., Mertens, S., & Weinheimer, C. 2013, *Advances in High Energy Physics*
- Emberson, J. D., Yu, H.-R., Inman, D., et al. 2017, *Research in Astronomy and Astrophysics*, 17, 085
- Euclid Collaboration, Knabenhans, M., Stadel, J., et al. 2018, [arXiv:1809.04695 \[astro-ph\]](#), [arXiv:1809.04695 \[astro-ph\]](#)
- Font-Ribera, A., McDonald, P., Mostek, N., et al. 2014, *Journal of Cosmology and Astro-Particle Physics*, 05, 023
- Foreman, S., Coulton, W., Villaescusa-Navarro, F., & Barreira, A. 2019, *arXiv e-prints*, 1910, [arXiv:1910.03597](#)
- Forero, D. V., Tórtola, M., & Valle, J. W. F. 2014, *Physical Review D*, 90, 093006
- Fukuda, Y., Hayakawa, T., Ichihara, E., et al. 1998, *Physical Review Letters*, 81, 1562
- Gagrani, P., & Samushia, L. 2017, *Monthly Notices of the Royal Astronomical Society*, 467, 928
- Gao, L., Springel, V., & White, S. D. M. 2005, *Monthly Notices of the Royal Astronomical Society*, 363, L66
- Gerbino, M. 2018, *arXiv e-prints*, [arXiv:1803.11545](#)
- Gonzalez-Garcia, M. C., Maltoni, M., & Schwetz, T. 2016, *Nuclear Physics B*, 908, 199
- Gualdi, D., Gil-Marín, H., Manera, M., Joachimi, B., & Lahav, O. 2019a, *Monthly Notices of the Royal Astronomical Society: Letters*, [arXiv:1901.00987](#)
- Gualdi, D., Gil-Marín, H., Schuhmann, R. L., et al. 2019b, *Monthly Notices of the Royal Astronomical Society*, 484, 3713
- Gualdi, D., Manera, M., Joachimi, B., & Lahav, O. 2018, *Monthly Notices of the Royal Astronomical Society*, 476, 4045
- Guo, H., Zheng, Z., Zehavi, I., et al. 2015a, *Monthly Notices of the Royal Astronomical Society*, 453, 4368
- . 2015b, *Monthly Notices of the Royal Astronomical Society*, 446, 578
- Hadzhiyska, B., Bose, S., Eisenstein, D., Hernquist, L., & Spergel, D. N. 2020, *Monthly Notices of the Royal Astronomical Society*, 493, 5506
- Hahn, C., Tinker, J. L., & Wetzel, A. 2019, [arXiv:1910.01644 \[astro-ph\]](#), [arXiv:1910.01644 \[astro-ph\]](#)
- Hahn, C., Villaescusa-Navarro, F., Castorina, E., & Scoccimarro, R. 2020, *Journal of Cosmology and Astroparticle Physics*, 03, 040
- Hamilton, A. J. S., Rimes, C. D., & Scoccimarro, R. 2006, *Monthly Notices of the Royal Astronomical Society*, 371, 1188
- Harker, G., Cole, S., Helly, J., Frenk, C., & Jenkins, A. 2006, *Monthly Notices of the Royal Astronomical Society*, 367, 1039
- Harnois-Déraps, J., van Waerbeke, L., Viola, M., & Heymans, C. 2015, *Monthly Notices of the Royal Astronomical Society*, 450, 1212
- Heavens, A. 2009, [arXiv:0906.0664 \[astro-ph\]](#), [arXiv:0906.0664 \[astro-ph\]](#)
- Heitmann, K., Higdon, D., White, M., et al. 2009, *The Astrophysical Journal*, 705, 156
- Hockney, R. W., & Eastwood, J. W. 1981, *Computer Simulation Using Particles*
- Jungman, G., Kamionkowski, M., Kosowsky, A., & Spergel, D. N. 1996, *Physical Review D*, 54, 1332



- Karagiannis, D., Lazanu, A., Liguori, M., et al. 2018, *Monthly Notices of the Royal Astronomical Society*, 478, 1341
- Kwan, J., Heitmann, K., Habib, S., et al. 2015, *The Astrophysical Journal*, 810, 35
- Lacerna, I., Padilla, N., & Stasyszyn, F. 2014, *Monthly Notices of the Royal Astronomical Society*, 443, 3107
- Lange, J. U., van den Bosch, F. C., Zentner, A. R., et al. 2019, arXiv:1909.03107 [astro-ph], arXiv:1909.03107 [astro-ph]
- Lazanu, A., & Liguori, M. 2018, *Journal of Cosmology and Astro-Particle Physics*, 2018, 055
- Leauthaud, A., Tinker, J., Bundy, K., et al. 2012, *The Astrophysical Journal*, 744, 159
- Lesgourgues, J., & Pastor, S. 2012
- . 2014
- Li, Y., Schmittfull, M., & Seljak, U. 2018, *Journal of Cosmology and Astro-Particle Physics*, 2018, 022
- Liu, A., Pritchard, J. R., Allison, R., et al. 2016, *Physical Review D*, 93, 043013
- Mandelbaum, R., Seljak, U., Kauffmann, G., Hirata, C. M., & Brinkmann, J. 2006, *Monthly Notices of the Royal Astronomical Society*, 368, 715
- Marulli, F., Carbone, C., Viel, M., Moscardini, L., & Cimatti, A. 2011, *Monthly Notices of the Royal Astronomical Society*, 418, 346
- McClintock, T., Rozo, E., Becker, M. R., et al. 2018, arXiv:1804.05866 [astro-ph], arXiv:1804.05866 [astro-ph]
- More, S., van den Bosch, F. C., Cacciato, M., et al. 2011, *Monthly Notices of the Royal Astronomical Society*, 410, 210
- Navarro, J. F., Frenk, C. S., & White, S. D. M. 1997, *The Astrophysical Journal*, 490, 493
- Peacock, J. A., & Smith, R. E. 2000, *Monthly Notices of the Royal Astronomical Society*, 318, 1144
- Petracca, F., Marulli, F., Moscardini, L., et al. 2016, *Monthly Notices of the Royal Astronomical Society*, 462, 4208
- Planck Collaboration, Aghanim, N., Akrami, Y., et al. 2018, arXiv:1807.06209 [astro-ph], arXiv:1807.06209 [astro-ph]
- Reischke, R., Desjacques, V., & Zaroubi, S. 2019, arXiv:1909.03761 [astro-ph], arXiv:1909.03761 [astro-ph]
- Rodríguez-Torres, S. A., Chuang, C.-H., Prada, F., et al. 2016, *Monthly Notices of the Royal Astronomical Society*, 460, 1173
- Rodríguez-Torres, S. A., Comparat, J., Prada, F., et al. 2017, *Monthly Notices of the Royal Astronomical Society*, 468, 728
- Saito, S., Takada, M., & Taruya, A. 2008, *Physical Review Letters*, 100, 191301
- . 2009, *Physical Review D*, 80, 083528
- Sartoris, B., Biviano, A., Fedeli, C., et al. 2016, *Monthly Notices of the Royal Astronomical Society*, 459, 1764
- Scoccimarro, R. 2015, *Physical Review D*, 92, arXiv:1506.02729
- Scoccimarro, R., Sefusatti, E., & Zaldarriaga, M. 2004, *Physical Review D*, 69, 103513
- Sefusatti, E., Crocce, M., Pueblas, S., & Scoccimarro, R. 2006, *Physical Review D*, 74, arXiv:astro-ph/0604505
- Sefusatti, E., Crocce, M., Scoccimarro, R., & Couchman, H. M. P. 2016, *Monthly Notices of the Royal Astronomical Society*, 460, 3624
- Sefusatti, E., & Komatsu, E. 2007, *Physical Review D*, 76, 083004
- Sefusatti, E., & Scoccimarro, R. 2005, *Physical Review D*, 71, arXiv:astro-ph/0412626
- Seljak, U. 2000, *Monthly Notices of the Royal Astronomical Society*, 318, 203
- Sheth, R. K., & Tormen, G. 2004, *Monthly Notices of the Royal Astronomical Society*, 350, 1385
- Song, Y.-S., Taruya, A., & Oka, A. 2015, *Journal of Cosmology and Astro-Particle Physics*, 2015, 007
- Springel, V. 2005, *Monthly Notices of the Royal Astronomical Society*, 364, 1105
- Takada, M., & Hu, W. 2013, *Physical Review D*, 87, 123504
- Tegmark, M., Taylor, A. N., & Heavens, A. F. 1997, *The Astrophysical Journal*, 480, 22
- Tellarini, M., Ross, A. J., Tasinato, G., & Wands, D. 2016, *Journal of Cosmology and Astro-Particle Physics*, 2016, 014
- Tinker, J. L., Leauthaud, A., Bundy, K., et al. 2013, *The Astrophysical Journal*, 778, 93
- Upadhye, A., Kwan, J., Pope, A., et al. 2016, *Physical Review D*, 93, 063515
- Vakili, M., & Hahn, C. 2019, *The Astrophysical Journal*, 872, 115



- van Daalen, M. P., McCarthy, I. G., & Schaye, J. 2020, *Monthly Notices of the Royal Astronomical Society*, 491, 2424
- Verde, L. 2010, [arXiv:0911.3105 \[astro-ph\]](#), 800, 147
- Viel, M., Haehnelt, M. G., & Springel, V. 2010, *Journal of Cosmology and Astro-Particle Physics*, 06, 015
- Villaescusa-Navarro, F., Banerjee, A., Dalal, N., et al. 2018, *The Astrophysical Journal*, 861, 53
- Villaescusa-Navarro, F., Bird, S., Peña-Garay, C., & Viel, M. 2013, *Journal of Cosmology and Astro-Particle Physics*, 2013, 019
- Villaescusa-Navarro, F., Hahn, C., Massara, E., et al. 2019, [arXiv:1909.05273 \[astro-ph\]](#), [arXiv:1909.05273 \[astro-ph\]](#)
- Wadekar, D., & Scoccimarro, R. 2019, [arXiv e-prints](#), 1910, [arXiv:1910.02914](#)
- Wang, H., Mo, H. J., & Jing, Y. P. 2009, *Monthly Notices of the Royal Astronomical Society*, 396, 2249
- Wechsler, R. H., Zentner, A. R., Bullock, J. S., Kravtsov, A. V., & Allgood, B. 2006, *The Astrophysical Journal*, 652, 71
- Wibking, B. D., Salcedo, A. N., Weinberg, D. H., et al. 2019, *Monthly Notices of the Royal Astronomical Society*, 484, 989
- Wolz, L., Kilbinger, M., Weller, J., & Giannantonio, T. 2012, *Journal of Cosmology and Astroparticle Physics*, 2012, 009
- Wong, Y. Y. Y. 2008, *Journal of Cosmology and Astroparticle Physics*, 2008, 035
- Yamauchi, D., Yokoyama, S., & Takahashi, K. 2017, *Physical Review D*, 95, 063530
- Yankelevich, V., & Porciani, C. 2019, *Monthly Notices of the Royal Astronomical Society*, 483, 2078
- Zennaro, M., Bel, J., Villaescusa-Navarro, F., et al. 2017, *Monthly Notices of the Royal Astronomical Society*, 466, 3244
- Zentner, A. R., Hearin, A., van den Bosch, F. C., Lange, J. U., & Villarreal, A. 2016, [arXiv:1606.07817 \[astro-ph\]](#), [arXiv:1606.07817 \[astro-ph\]](#)
- Zhai, Z., Tinker, J. L., Becker, M. R., et al. 2019, *The Astrophysical Journal*, 874, 95
- Zheng, Z., Coil, A. L., & Zehavi, I. 2007, *The Astrophysical Journal*, 667, 760
- Zheng, Z., Berlind, A. A., Weinberg, D. H., et al. 2005, *The Astrophysical Journal*, 633, 791
- Zu, Y., & Mandelbaum, R. 2015, *Monthly Notices of the Royal Astronomical Society*, 454, 1161